I COMPUTATIONAL METHOD

To reduce the computational cost, only a symmetrical section of the power block is modelled. The full details of steady state governing differential equations of fluid flow in the pipes and heat conduction in pipe graphite walls and insulation can be found elsewhere[1]. For details on Monte Carlo Ray Tracing (MCRT) the reader is referred to Howell and Siegel [2] and Haji-Sheikh and Howell [3]. Solution of the governing equations consists of iteration between two steps. First the radiative heat flow between the emitter and TPV cell is calculated by MCRT. Second, the temperature and heat flux distributions throughout the insulation and pipe walls are calculated by solving the conjugate heat transfer problem subject to the MCRT results as an input heat flux. For a prescribed radiative heat flux distribution on the surface of the TPV cell and emitter, the 3D Navier Stokes, energy, and turbulence equations were solved simultaneously with the heat conduction equations in tube walls and insulation using the Finite Volume Method (FVM) based on a collocated grid system. The resulting temperature profile is then used to update the MCRT calculation and the iteration between the two steps proceeds until convergence. The MCRT calculation is considered converged when the maximum value of relative error in both temperature and heat flux on the TPV cell surface is $\leq 10^{-6}$. The FVM calculation is considered converged when the residuals for the continuity, momentum, energy and turbulent equations are $\leq 10^{-5}, 10^{-6}, 10^{-8}$, 10^{-6}, respectively. The Relative Error (RE) in FVM procedure is defined as

$$RE = \sum_{cells} \left| \frac{\varphi^{n+1} - \varphi^{n}}{\varphi^{n}} \right| \tag{1}$$

Where the superscript n refers to the previous iteration and φ represents velocity components, temperature, and other scalars. The overall energy balance in the entire system is checked as a second criterion for convergence as well. For details about the numerical method used to solve Navier Stokes and turbulent equations please see the work of Peyret[1].

A combination of wall, inlet, outlet, and symmetry boundary conditions were applied to the computational domain. The inner surfaces of tubes which are in contact with the LMHTF are treated with a no-slip boundary condition, i.e., zero velocity components ($u = v = w = 0$). Constant temperature and uniform velocity profiles were applied as boundary conditions at the tube inlets. At the solid-liquid interface, both heat transfer and temperature continuity is enforced. i.e., $T_{solid} = T_{liquid}$, $k_{solid} \frac{\partial T_{solid}}{\partial n} = k_{liquid} \frac{\partial T_{liquid}}{\partial n}$, where n is a vector normal to surface and k is thermal conductivity. At the symmetry surface, the gradient of all variables are set to zero, i.e., $\frac{\partial \varphi}{\partial n} = 0$. At the outlet, the static pressure is fixed and the remaining flow variables are extrapolated from the interior of the domain, i.e., $\frac{\partial \varphi}{\partial n} = 0$. The external surfaces of the power block are in contact with surroundings at room temperature (300K) through both radiative and convective cooling. It is assumed that the TPV cell is cooled by a heat sink to a desired cell temperature (T_c). The internal surfaces of insulation are assumed diffuse and the surface of the graphite tube emitters are treated as diffuse while frequency dependent specularity and reflectivity were considered for the TPV cell allowing the edge effects to be captured. Band gap is function of cell temperature, the temperature dependent band gap is used for $Ga_xIn_{1-x}As$ [4]

$$E_g(x,T) = 0.42 + 0.625x - \left[\frac{5.8}{(T+300)} - \frac{4.19}{(T+271)} \right].10^{-4}T^2 x - 4.19 T^2 / (T+271) + 0.475x^2 \tag{2}$$

Where T is cell temperature in Kelvin and E_g is band gap energy in electron volts.

We studied the effect of the size of the system by changing the number of tubes and insulation thickness. To obtain better accuracy in the simulations and grid sensitivity, for each case, four tetrahedral meshes were generated by discretizing the computational domain and the results were compared to determine the best grid. Sufficiently fine grids are used near the wall to accurately capture the temperature and velocity gradients. In the MCRT method, the number of cells on the surfaces of optical cavity is controlled to contain roughly the same number of particles to have similar

statistical variation. It was found that around 45 particles per computational cell on average is enough to resolve radiation field on the TPV cells and graphite emitter. Furthermore, the effect of the number of particles in the optical cavity were studied and it was found that depending on the size of optical cavity roughly $400,000 - 1,000,000$ particles are sufficient to capture the radiation distribution on the surfaces of optical cavity. Therefore, $400,000 - 1,000,000$ photon bundles are traced per MCRT iteration, i.e., the outer loop iteration and the mean temperature of each cell is fed back to the FVM to solve for the temperature distribution in the liquid and solid regions of the computational domain. It was found that tracing more photon bundles per time step did not change the simulation results, but significantly increased the computational time.

In order to calculate the output electrical energy from the system, the input radiation is super imposed over the External Quantum Efficiency (EQE) curve of PV cell. EQE measures the efficiency with which the cell can convert the incident radiation into electricity. The generated current from the cell can be calculated by multiplying the EQE with input radiation spectrum and integrating over the entire range of wavelength and surface of PV cell

$$I(x,y,z) = e \int_0^{\lambda_g} \frac{Q(x,y,z,\lambda)}{hc/\lambda} EQE(\lambda) \, d\lambda \tag{3}$$

Where e is electron charge, $Q(x,y,z,\lambda)$ is the spectral irradiation distribution to the PV cell from the graphite emitter, h is Planck constant, c is light velocity, λ_g is wavelength corresponds to band gap energy, and EQE is the external quantum efficiency of cell. In Eq. 3, $\frac{Q(x,y,z,\lambda)}{hc/\lambda}$ represents the number of photons incident on the TPV cell with wavelength λ. To consider a more realistic case, a polynomial curve is fitted to experimental EQE curve of an InGaAs (η_{cell} = 12.4%) cell used by Tuley et al.,[5]

$$EQE(\lambda) = a_0 + a_1\lambda + a_2\lambda^2 + a_3\lambda^3 + a_4\lambda^4 + a_5\lambda^5 \tag{4}$$

Where $a_0 - a_5$ are fitting curve coefficients. The total light generated current is then calculated as follows

$$I_L = \frac{1}{A_{\text{mod}}} \int I(x,y,z) \, dA_{cell} \tag{5}$$

where A_{mod} is the area of TPV module in front of graphite emitter.

Two different sets of assumptions are made about the cell performance in order to illustrate where the current technology is, and how much room for improvement exists. For the first case, all the recombination and series resistance losses are considered in the calculation by using the experimental data for series resistance and wavelength dependent EQE, as well as ideal and non-ideal dark current saturations[5]. For the second case the only loss mechanism assumed in the calculation is radiative recombination and resistive loss due to series resistance in the cell. Series resistance is very important at high injections such as the TPV system studied in this paper, therefore considering its effect is crucial. The calculation of the open-circuit voltage and fill factor for each case is explained below.

Case I (Real cell $EQE \neq 1, V_{oc} \neq V_{\text{max}}$**):** For this case a two diode model of a TPV cell was used to consider the effect recombination in the cell and non-ideal saturation current in space charge region.

$$I = I_L - I_{01}\left(e^{qV+R_sI/n_1k_BT} - 1\right) - I_{02}\left(e^{qV+R_sI/n_2k_BT} - 1\right) - \frac{V+R_sI}{R_{SH}} \tag{6}$$

Where I and V are the terminal current and voltage, respectively. I_L is photocurrent, I_{01} and I_{02} are the ideal dark saturation current and space charge non-ideal dark saturation component, respectively. R_s, R_{SH}, n_1 and n_2 are series

resistance, shunt resistance, and ideality factor of diffusion and recombination diodes, respectively. n_1 is often assumed to be equal to 1 by many authors, in accordance with the diffusion theory of p-n junctions[6], whereas n_2 is sometimes set equal to 2, in accordance with the theory of recombination via traps[7]. The value of I_{01} and I_{02} can be obtained either by using two diode model in conjunction with experimental value of R_s, R_{SH}, V_{oc}, I_{SC} and FF reported by Tuley et al[5] or by directly fitting to the experimental current voltage curve. Therefore, the calculation of V_{oc}, I_{SC} and consequently all of the efficiencies calculated in this paper consider the recombination in the cell and resistive losses due to series resistance. The shunt resistance is neglected in the calculation due to the high level of injection studied in this paper. Furthermore, since the shunt resistances are largely dependent on the quality of cell fabrication, and it is common to fabricate cells with high shunt resistance, the shunt resistance losses can be safely neglected.

At the open circuit voltage $V = V_{oc}$, the current $I = 0$, therefore,

$$I_L = I_{01}\left(e^{qV_{oc}/n_1 k_B T} - 1\right) + I_{02}\left(e^{qV_{oc}/n_2 k_B T} - 1\right) + \frac{V_{oc}}{R_{SH}} \tag{7}$$

Eq. 7 is solved numerically to obtain the open-circuit voltage. The maximum power point can be calculated by differentiating Eq. 7 with respect to voltage, i.e., $\frac{dI}{dV} = 0$ and consequently the numerical solution of the resulting equation is used to obtain the current and voltage corresponding to the maximum power, i.e., I_m and V_m. Finally the fill factor is calculated as follow

$$FF = \frac{I_m V_m}{I_{Sc} V_{oc}} \tag{8}$$

Case 2 (fundamental efficiency limit $EQE = 1, V_{oc} = V_{max}$**):** For this case the maximum fundamental limit of open-circuit voltage is obtained by only considering radiative recombination in the TPV cell. Kiess and Rehwald[8] based on thermodynamic considerations give the following limit for open-circuit voltage at any non-zero cell temperature.

$$eV_{max} = E_g + k_B T \ln\left(\left(\frac{h^3 c^2}{2\pi k_B T}\right)\left(\frac{I_{SC}}{e E_g^2}\right)\right) \tag{9}$$

Where k_B is Boltzmann constant, T is cell temperature, I_{sc} is short-circuit current. Equation 9 calculates the maximum limit of open-circuit voltage at any cell temperature. The fill factor is calculated using the empirical equation derived by Green[9]

$$FF_{max} = \frac{v_{max} - \ln(v_{max} + 0.72)}{v_{max} + 1} \tag{10}$$

where v_{OC} is defined as normalized maximum open-circuit voltage, i.e, $v_{max} = \frac{eV_{max}}{k_b T}$.

The effect of the series and shunt resistances can be incorporated in the calculation by defining normalized series and shunt resistances resistance as

$$r_S = \frac{R_S}{V_{max}/I_{SC,max}} \tag{11}$$

$$r_{SH} = \frac{R_{SH}}{V_{max}/I_{SC,max}} \tag{12}$$

Therefore, the modified fill factor for this case, i.e., $EQE = 1, V_{oc} = V_{max}$ is calculated using following equation[10]

$$FF'_{max} = FF_{max}(1-r_S)\left[1 - \frac{(v_{max}+0.7)}{v_{max}}\frac{FF_{max}(1-r_S)}{r_{SH}}\right] \tag{13}$$

The electrical power and overall efficiency of system can be calculated using Fill Factor (FF), which is the ratio of maximum possible power obtained from the cell to the product of open-circuit voltage and short-circuit current density.

$$P = \begin{cases} N_{cell}V_{OC}I_{SC}FF & EQE \neq 1, V_{oc} \neq V_{amx} \\ N_{cell}V_{max}I_{SC,max}FF'_{max} & EQE = 1, V_{oc} = V_{amx} \end{cases} \tag{14}$$

$$\eta = \frac{P - W_{cooling}}{Q_{in}} \tag{15}$$

Where N_{cell} is number of PV cells in the entire power block, $W_{cooling}$ is the pumping power needed by thermal management system, and Q_{in} is total energy input to the system, which is the sensible heat transferred from liquid metal heat transfer fluid (LMHTF) to the graphite tubes

$$Q_{in} = \sum_{i=1}^{N} \dot{m}_i C_p \left(T_{out} - T_{in}\right)_i \tag{16}$$

Where $\dot{m}_i$ is mass flow rate of LMHTF in pipes, C_p is specific heat, $(T_{out} - T_{in})$ is temperature difference between inlet and outlet, and N is number of tubes in the system.

The validation of MCRT code was performed with respect to numerical results presented by Wierelt and Ruo[11] for right circular cylinders to rectangular planes and as shown in Figure S1 good agreement was observed with their results.
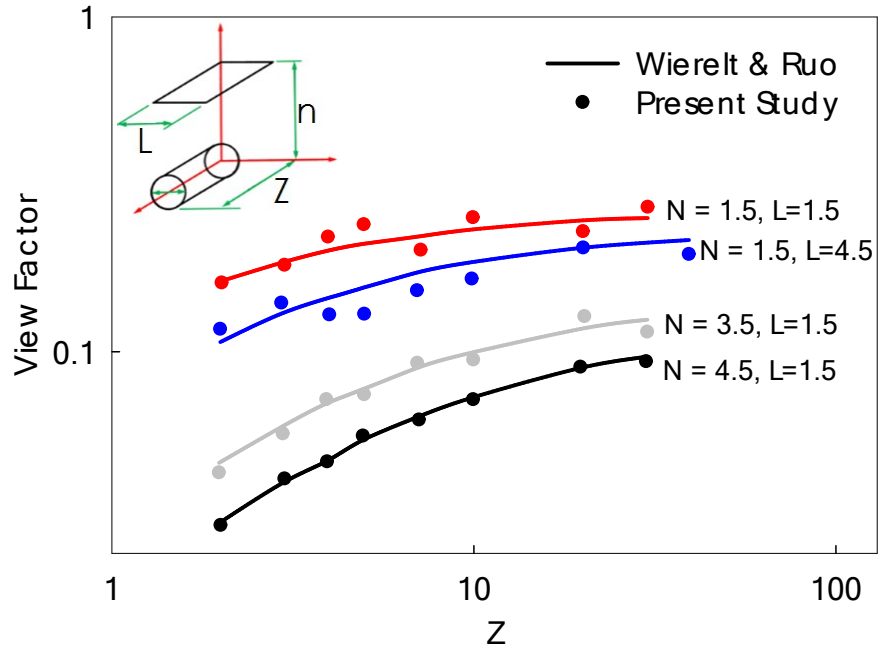
Figure S1: Comparison of view factor obtained using our model and literature data

The FVM code is validated by comparing the results predicted by our code against experimental correlations[12, 13] for turbulent flow of liquid metal in circular pipes with constant heat flux boundary condition as well as numerical simulation of turbulent flow conducted by Ji and Gardner[14]. As seen in Fig S2 our results underpredict the experimental Nusselt number but they are reasonable if one considers the limits of experimental uncertainty in the data used to determine the correlation. Moreover, it can be seen that our results are closer to experimental data compared to numerical results of Ji and Gardner[14]. This is due to the different turbulent parameters used in our work and their work. Furthermore, since the convective heat transfer coefficient for the LMHTF is non limiting, all of the results are insensitive to the differences in Nusselt number, which vary by ~ 20%.
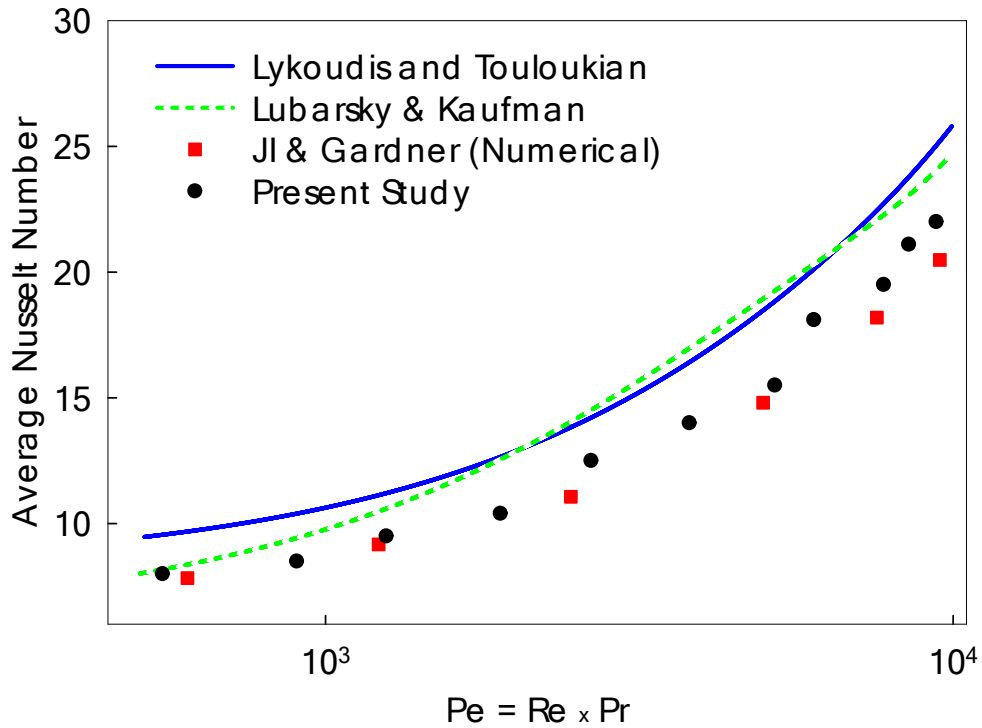
Figure S2: Comparison of average Nusselt number obtained using our model and literature data

II SIZE EFFECTS ON POWER BLOCK EFFICIENCY

The edge effects depend on the aspect ratio of the optical cavity. Intuitively the larger the aspect ratio, the smaller the edge effects, but it is not clear a *priori* how large of an aspect ratio is needed before the effects become negligible. The effect of non-uniform illumination on the surface of TPV cells (e.g., edge effects) for two example systems with different aspect ratios is shown in Fig. S3. As seen for the system with a lower height to width ratio, the heat flux is low near the edges due to a lower view factor between the edges and the emitter. For the larger height to width ratio system the edge effects are less significant, which results in more uniform radiation and consequently higher efficiency. It can also be seen that using circular pipes still results in a rather uniform illumination on the surface of the TPV cells, which is advantageous, because circular pipes are less expensive and more straightforward to fabricate than flat plates, square tubes, or a concentric design which would likely yield the most uniform illumination. It is important to mention that the overall efficiency of power block is function of its volume to surface area ratio, because the heat loss to the environment and power output are proportional to surface area and volume, respectively. Therefore, the length scale in which heat loss is minimized is function of both insulation thickness and size of optical cavity. In order to obtain the length scale, we first identified the aspect ratio beyond which, the edge effects on radiation in the optical cavity become negligible

by MCRT simulation of radiation between emitter and TPV cell for different length, height and distance between emitter and TPV cell. Figure S4 shows the effect of aspect ratios of the system on the heat fluxes on the surface of the TPV cells. The values are normalized by their maximum values on the surface. It can be seen that increasing the aspect ratios, i.e, $AR_H = H/C$ and $AR_L = L/C$ of the system (e.g., ratio between overall height of system (H) to distance between cell and tubes (C), and the ratio between overall length of system (L) between cell and tubes) beyond AR_H and AR_L = 40 and 60, minimally changes the heat flux as compared to the asymptotic limit.
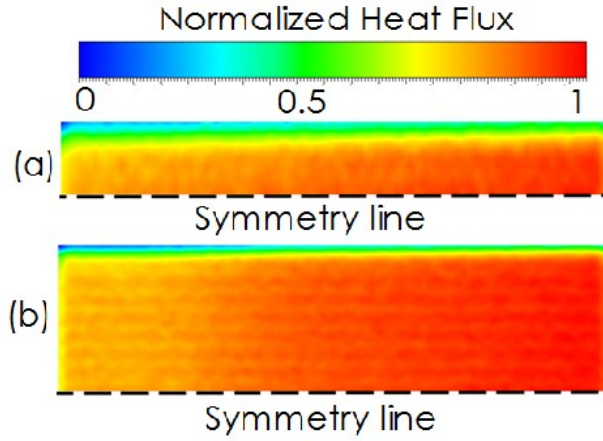
Fig S3. Normalized in band heat flux on PV cell, (a) two pipes (H=2D), (b) eight pipes (H=8D)
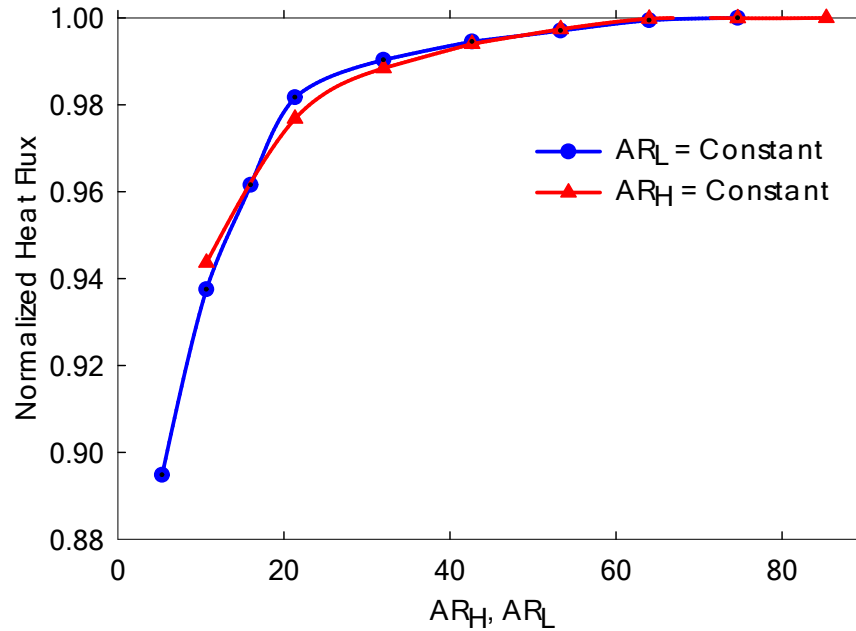
Fig S4. Normalized in band and out of band heat fluxes on PV cell vs aspect ratios

III   TPV CELL THERMAL MANAGEMENT

Two types of heat sinks are studied (1) an array of circular tubes and (2) a copper pin fin structure. Both are water cooled heat sinks used to cool the TPV cells and in both cases the coolant flows parallel to TPV cells at a specified temperature and velocity at the inlet channel. Thus, the water temperature increases as it moves through the heat sink and reaches the maximum temperature at the outlet. Different geometries for tube cross sections and pin fins can be used, but in the present study, the circular tube and pin fin were adopted due to their wide availability. Thus, we expect the heat sink cost to be negligible to the system cost. The total height and width of both heat sinks are 1 m. For the circular tube heat sink, the diameter of the tube is 9 cm and the distance between the tubes is 0.05 cm. For the pin fin heat sink, a staggered arrangement with 14 fins along the coolant flow direction is used. The diameter of fins and distance between their centers are 2.3 cm and 7 cm, respectively. Because of the symmetrical geometry of heat sinks, only one symmetrical part of them is selected and used in the computation. For the pin-fin heat sink the computational domain contains three rectangular volumes, one representing the flow developing inlet block with a length nearly 5 times the hydraulic diameter of pin cross-section, the other is outlet block with a length nearly 14 times the hydraulic diameter of pin cross-section which was created in order to avoid any influence of the eventual back flow streams on the final results. The third is the central region which contains the pins and heated wall. The height of all domains is similar to height of the pins. It is assumed the coolant flow is incompressible and the thermophysical properties of copper and water are temperature dependent.

A constant and uniform velocity and temperature is applied at the inlet of computational domain. A constant heat flux is applied at the bottom wall of the heat sinks where it is attached to TPV cell. It is important to note that in this calculation, a worst case scenario is assumed, whereby all of the photons with energy above and below band gap are absorbed in the cell and generate heat in the cell/module and only photons with energy equal to bandgap are converted to electricity. This is the worst heating case scenario that can happen in the systems because (1) in the real device a portion of photons with energy below bandgap of TPV cell will be transmitted through the device and will be reflected back to the emitter via the back surface reflector (BSR), and will therefore not contribute much to the heat generation, (2) In our calculation it is assumed that the size of array of TPV modules is $1 m^2$ which is larger than the size required for convergence of the efficiency with respect to system size (~0.4 m²). The large size of TPV cell results in less heat removal from the system and consequently more heat accumulation in the cell, through the higher water temperature rise. (3) In the case of a multijunction TPV cell, since the photons with energy above bandgap are distributed between the number of junctions, the thermalization losses and consequently the heat generation is significantly lower than a single junction cell. Therefore, using a single bandgap cell results in maximum heat generation of heat in the cell. Therefore, the maximum possible heat flux from the array of TPV modules is prescribed as the heat flux boundary condition on the bottom wall of heat sink, via

$$Q_{max} = \int_0^\infty E \cdot n(\lambda, T_E, 0, \Omega_{abs}) dE - \int_{E_g}^\infty E_g \cdot n(\lambda, T_E, 0, \Omega_{abs}) dE \qquad (17)$$

Where $n(\lambda, T_E)$ is photon emission flux per energy interval (dE) per unit solid angle (Ω)

$$n(E, T, \mu, \Omega) = \frac{2\Omega}{c^2 h^3} \frac{E^2}{e^{\left(\frac{E-\mu}{k_b T}\right)} - 1} \qquad (18)$$

Where T_E is the temperature of graphite tubes, h is Planck's constant and k_b is the Boltzmann's constant. In the case of thermal emission such as emission from graphite tubes the chemical potential is zero, i.e., $\mu = 0$.

The temperature distributions in the heat sinks are shown in Fig. S5. Clearly, at the channel inlet the temperature of the coolant is originally uniform but it changes due to the interaction with slightly warmer surfaces. As seen, with increasing inlet velocity of water the temperature distribution changes and the thermal boundary layer thicknesses on the fins and tube surfaces decrease. Therefore, the heat transfer from warmer surfaces to water increases and the average

temperatures of warmer surfaces attached to the TPV module array decreases. It is important to mention that possible mismatch losses in the TPV module are due to either non uniform temperature or non-uniform illumination on the cells. Since the temperature of the LMHTF in the graphite tubes decreases from inlet to outlet by about 20 K, the TPV module arrays see a slightly different spectrum along the tubes length. As a result, the module arrays experience have slightly different power outputs. To solve this issue, the direction of water flow in the thermal management system can be same of the direction of liquid metal in the graphite pipes. Therefore, the TPV cells with higher temperature experiences more cooling consequently more temperature uniformity can be obtained throughout the module. The second source of mismatch can be due to non-uniform and variable illumination on the cells due to size effect but it can be minimized significantly for large system. For larger system sizes, the edge effects become negligible and hence the illumination become more uniform on the surface of TPV module.
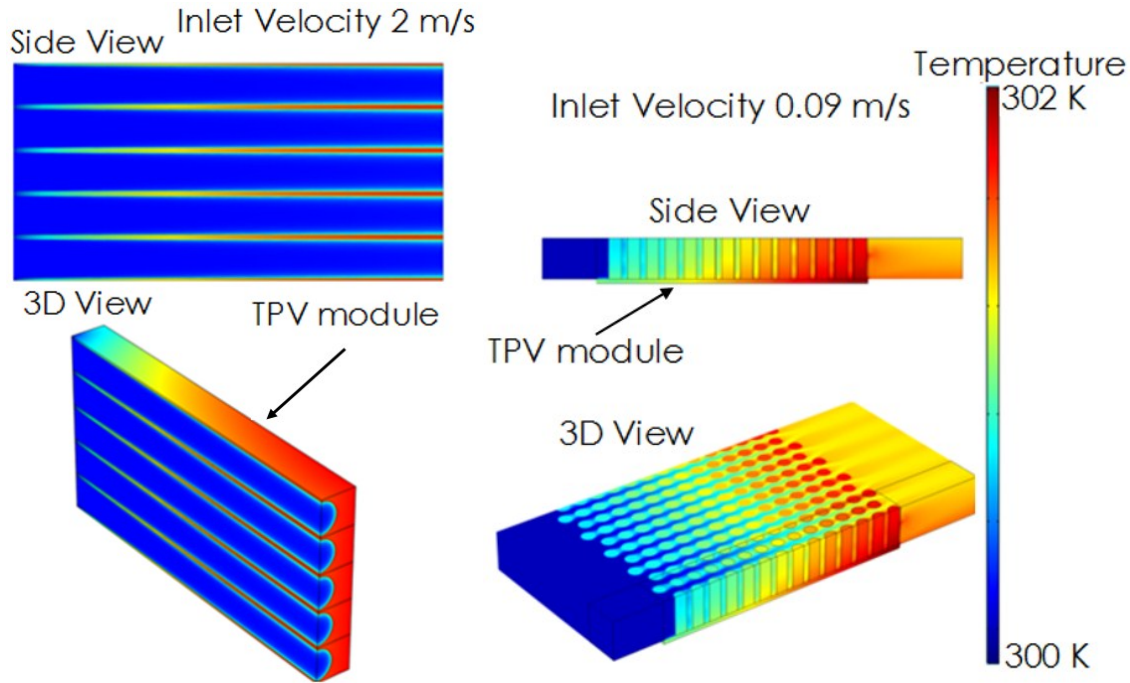
Figure S5: Two conventional liquid-cooled copper heat sinks to cool the TPV cells

The above results show that liquid-cooled conventional heat sinks can remove the heat from TPV cells efficiently with low fabrication cost. The only concerning issue is the pumping power necessary to pump the liquid to the heat sink. The parasitic load depicted in Fig. S6. As seen, the parasitic load increases with the inlet velocity but the maximum temperature of base plate decreases. It can be seen that the pumping power required to pump water in the heat sink is not significant compared to the power generated by TPV module array therefore the overall efficiency of the system is not sensitive to pumping power.
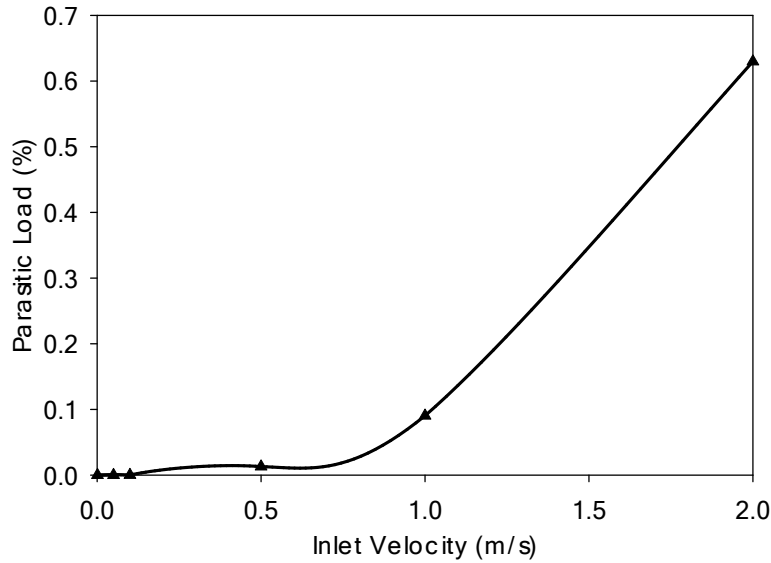
Figure S6: Pumping power versus inlet velocity of liquid in circular tubes heat sinks

IV REFERENCES

1.   R. Peyret, *Handbook of computational fluid mechanics*, Academic Press, 1996.
2.   R. Siegel and J. Howell, *Hemisphere, New York*.
3.   A. Haji-Sheikh and J. Howell, *Handbook of Numerical Heat Transfer, Second Edition*, 1988, 249-295.
4.   S. Paul, J. Roy and P. Basu, *Journal of applied physics*, 1991, **69**, 827-829.
5.   R. S. Tuley, J. M. S. Orr, R. J. Nicholas, D. C. Rogers, P. J. Cannard and S. Dosanjh, *Semiconductor Science and Technology*, 2013, **28**, 015013.
6.   V. Aubry and F. Meyer, *Journal of Applied Physics*, 1994, **76**, 7973-7984.
7.   M. Veerachary, T. Senjyu and K. Uezato, *Ieee Transactions on Aerospace and Electronic Systems*, 2002, **38**, 262-270.
8.   H. Kiess and W. Rehwald, *Solar Energy Materials and Solar Cells*, 1995, **38**, 45-55.
9.   M. A. Green, *Solid-State Electronics*, 1981, **24**, 788-789.
10. M. A. Green, *Solar cells : operating principles, technology and system applications* Prentice-Hall, Inc, Englewood Cliffs, NJ, 1992.
11. J. A. Wiebelt and S. Y. Ruo, *International Journal of Heat and Mass Transfer*, 1963, **6**, 143-146.
12. B. Lubarsky and S. J. Kaufman, *NACA Tech. note 3336*, 1955.
13. P. S. Lykoudis and Y. S. Touloukian, *Transactions of the ASME*, 1958, 653-666.
14. H. C. Ji and R. A. Gardner, *International Journal of Heat and Mass Transfer*, 1997, **40**, 1839-1851.